JEM Journal of Experimental Medicine

BRIEF DEFINITIVE REPORT

Activated PIK3CD drives innate B cell expansion yet limits B cell–intrinsic immune responses

Michelle N. Wray-Dutra[1,2], Fahd Al Qureshah[1,2,5], Genita Metzler[1,2], Mohamed Oukka[1,2,3], Richard G. James[1,3,4], and David J. Rawlings[1,2,3]

Activated PI3K-delta syndrome (APDS) is an immunodeficiency caused by gain-of-function mutations in PIK3CD. This disease exhibits complex immune phenotypes including increased IgM, recurrent infection, and impaired vaccine responses. To better understand the impact of B cells in this disease, we generated an inducible model of the common APDS mutation (h*PIK3CD*-E1021K; referred to as aPIK3CD) and intercrossed these mice with B cell–specific Cre models. Mb1-aPIK3CD mice exhibited bone marrow B lymphopenia and, conversely, expansion of the peripheral innate B1a and MZ B cell compartments. aPIK3CD B cells manifest increased pS6 and increased survival at several stages, without alterations in cycling, and baseline increases in plasma cells, natural IgM, and IgG3. Finally, Mb1-aPIK3CD mice exhibited blunted T cell–independent immune responses, and both AID- and CD21-aPIK3CD mice displayed reduced class-switched antibodies following T cell–dependent immunization. Thus, aPIK3CD alters B cell development and function and is counter-productive during immune responses, providing insight into B cell–intrinsic contributions to the APDS phenotype.

Introduction

Phosphatidylinositol 3-kinase (PI3K) signaling plays a critical role at several stages of B cell development. Class 1A PI3K proteins function as heterodimers between catalytic (PIK3CA, B, and D) and regulatory (PIK3R1–3) subunits. These heterodimeric complexes catalyze phosphorylation of the 3-OH group of integral membrane phosphoinositides critical for the activation of downstream kinases that regulate B cell survival, differentiation, and metabolism, including, but not limited to, BTK, AKT, and MTOR.

The catalytic subunits of class 1A PI3Ks have overlapping expression patterns. PIK3CA and PIK3CB are expressed ubiquitously, whereas PIK3CD (p110δ) is restricted to immune cells. Despite the structural and expression similarities, loss-of-function studies have revealed that PIK3CD and its regulatory subunit PIK3R1 (p85) are the primary class 1A PI3K downstream of the B cell antigen receptor (BCR). While deletion of either gene in mice limits central B cell development, mature B cell development is also altered, resulting in development of fewer B1 and marginal zone (MZ) B cells (Jou et al., 2002). These cellular defects contribute to decreased immunoglobulin production, weak responses to T cell–independent (TI) antigens, and lack of response to T cell–dependent (TD) antigens in mice (Jou et al., 2002; Okkenhaug et al., 2002) or humans deficient in either PIK3CD (Zhang et al., 2013) or PIK3R1 (Conley et al., 2012). Conversely, B cell–specific activation of class 1A PI3Ks, as assessed using genetic models of PI3K hyper-activity, also leads to defects in both TI and TD responses. For example, deficiency of either the PI3K phosphatases, INPP5D (Liu et al., 1998; Okada et al., 1998) or PTEN (Browning et al., 2015), or forced expression of membrane-tethered PIK3CA (Sander et al., 2015), results in loss of B cell class-switch recombination and maturation in response to TD antigens.

As suggested from the data in mice, primary immunodeficiency in humans can be caused by germline mutations in PIK3CD (p110δ) or PIK3R1 (p85) that increase class 1A PI3K signaling. Patients with activating mutations in either gene present with complex immune phenotypes that include susceptibility to bacterial and viral respiratory infections, B cell lymphopenia, effector-memory T cell hyperplasia and senescence, antibody dysregulation (increased IgM and decreased IgG2), and acquisition of B cell lymphoma. The cell–intrinsic roles for B and T cells in this newly identified immune dysregulation disease, called activated PI3K-delta syndrome (APDS), have not been carefully elucidated. Here, we report an inducible murine model of APDS driven by a common activating mutation in PIK3CD (E1020K). Our data show that many aspects of the APDS clinical phenotype can be explained by B cell–intrinsic, activated PI3KD-driven signaling. Dysregulated PI3K signals in B cells lead to defects in immature B cell development, preferential expansion of innate-like B cells,

[1]Seattle Children's Research Institute, Seattle, WA; [2]Department of Immunology, University of Washington, Seattle, WA; [3]Department of Pediatrics, University of Washington, Seattle, WA; [4]Department of Pharmacology, University of Washington, Seattle, WA; [5]King Abdulaziz City for Science and Technology, Riyadh, Saudi Arabia.

Correspondence to David J. Rawlings: drawling@u.washington.edu.

increases in natural IgM, and a naive B cell compartment that lacks the capacity to respond appropriately to immune challenge.

Results and discussion

A cell-intrinsic model for tissue-specific knock-in of activated PIK3CD

To understand how activating mutations in the catalytic subunit of PIK3CD impact the differentiation and homeostasis of immune cells, we generated an inducible mouse model of PIK3CD-E1020K (equivalent to hE1021K, hereafter referred to as aPIK3CD). A targeting vector containing the aPIK3CD mutation within exon 24 of the *Pik3cd* gene and relevant Cre-loxp sites was introduced by homologous recombination into the endogenous *Pik3cd* locus. The mutant exon was placed in the opposite orientation of transcription (3′→5′) and downstream of the endogenous exon 24. Upon Cre-mediated excision, the endogenous exon 24 is excised and the mutant exon is flipped so that its transcription is subject to endogenous regulation (Fig. S1 A). Using droplet digital PCR (ddPCR) with knock-in (junction)–specific probes, we confirmed the flipping efficiency in $CD21^{Cre/+}aPIK3CD^{+/-}$ to be ∼50% and restricted to the B cell lineage, as expected in a heterozygote genotype (Fig. S1, B–D). These data demonstrate establishment of an efficient murine model that enables tissue-specific expression of aPIK3CD.

Expression of aPIK3CD in developing B cells leads to bone marrow (BM) B lymphopenia

APDS patients exhibit peripheral B cell lymphopenia (Angulo et al., 2013; Lucas et al., 2014, 2016; Dulau Florea et al., 2017; Wentink et al., 2017). BM B cell phenotyping in a limited number of APDS subjects has suggested that aPIK3CD may impact the pre–B-I stage, leading to an increased proportion of apoptotic $CD19^{dim}$ B cell progenitors (Wentink et al., 2017) or, similarly based on alternative surface markers, a proportional increase in $CD10^{hi}$ $CD20^{neg}$ early B cell progenitors (Dulau Florea et al., 2017). To better understand the consequences of hyperactive PI3K signaling during early B cell development, we crossed aPIK3CD animals to the Mb1-Cre strain to drive aPIK3CD expression beginning at the pro–B cell stage (Hobeika et al., 2006). To minimize the indirect effects of long-term aPIK3CD expression, we focused our analyses on cohorts 11–13 wk of age. As anticipated based upon biochemical analysis of primary T and B cells in APDS subjects (Angulo et al., 2013; Lucas et al., 2014; Wentink et al., 2017), all splenic B cells subsets displayed increased phosphorylation of ribosomal protein S6 (pS6; Ser235/236) compared with controls (Fig. 1, A and B). Mb1-aPIK3CD mice displayed diminished frequency and ∼50% reduction in the absolute number of BM B cells (Fig. 1, C and D; and Fig. S1 E). Detailed characterization of the BM B cell compartment demonstrated an increased proportion of pro–B cells ($B220^+IgM^-CD43^+$) and a decreased frequency of mature recirculating B cells ($B220^+IgM^+IgD^+$, Fig. 1 E and Fig. S1 E). By absolute cell counts, we observed a reduction in the number of small pre- and mature recirculating B cells (Fig. 1 F and Fig. S1 E). Thus, while previous human studies were unable to assess total BM B progenitor cell numbers, consistent with phenotypic data from APDS subjects, B cell–intrinsic aPIK3CD expression restricts BM B lymphopoiesis with its major impact at the pre-B stage leading to a proportional increase in pro–B cells and reduction in the absolute number of pre–B, immature, and recirculating B cells.

aPIK3CD expression promotes expansion of peripheral innate B cell compartments

We next evaluated the impact of aPIK3CD on peripheral B cell development. In the peritoneum, Mb1-aPIK3CD mice displayed increases in both the proportion and absolute number of B1a B cells (Fig. 1, G and H; and Fig. S1 F) and a proportional reduction in the frequency, but not the number, of B1b and B2 B cells. In the spleen, Mb1-aPIK3CD mice exhibited an increased proportion of MZ B cells and a decrease in the proportion of follicular mature (FM) B cells with a similar trend in cell numbers (Fig. 1, I and J; and Fig. S1 G). Thus, despite a reduction in BM B cell development, B cell–intrinsic aPIK3CD expression is sufficient to drive expansion of both the B1a and MZ B cell compartments.

aPIK3CD B cells exhibit differential selection within the immature versus MZ and B1a compartments

To precisely assess the specific stages of B cell development wherein cells expressing aPIK3CD exhibit altered competitive selection, we performed BM chimera studies using mixed populations of WT ($CD45.1^+$) and Mb1-aPIK3CD (aPIK3CD, $CD45.2^+$) BM transplanted into congenically marked, B cell–deficient μMT recipients ($CD45.1^+/CD45.2^+$). Recipient mice were characterized 12 wk after transfer to interrogate chimerism within B cell developmental stages. Within the BM, relative to aPIK3CD cells, WT B cells were enriched at the immature stage ($B220^+IgM^+IgD^-$), an advantage that remained despite skewing the input BM ratio to 2:1 in favor of aPIK3CD cells (Fig. 2, A and B). As the absolute number of immature B cells is primarily dependent on clonal expansion of pre–B cells, this reduced competitive fitness likely reflects the diminished small pre–B cell compartment (Fig. 1 F) observed under homeostatic conditions.

Similar to our observations in the periphery of Mb1-aPIK3CD mice, despite their being at a disadvantage before egress from the BM, aPIK3CD B cells outcompeted WT cells within the B1a (Fig. 2, C and D) and MZ compartments (Fig. 2, F and G). In addition to the impact on the B1a cells, we observed skewing in favor of aPIK3CD B1b B cells, suggesting that aPIK3CD globally promotes B1 B cell fitness, as evidenced by the elevated numbers of Mb1-aPIK3CD–derived B1a and B1b cells (Fig. 2 E), and enhances the activated B1a $CD5^+$ phenotype.

To determine whether aPIK3CD alters innate B cell populations independently of early B lineage commitment, we crossed aPIK3CD mice to the CD21-Cre strain. In this model, aPIK3CD is first expressed at the splenic T1 stage and to a somewhat lesser degree in peritoneal B cells (Martin and Kearney, 2001). CD21-aPIK3CD displayed an expansion of innate B cells, including an increased frequency of B1a cells, with a trend toward increased numbers (Fig. 2, H and I), and significant increases in MZ B cell numbers with a concomitant decrease in FM B cells (Fig. 2, J and K). While chimeric studies suggested a trend for increased proportion of aPIK3CD transitional B cells (Fig. 2 G), absolute numbers of T1/T2 and MZ precursor (MZp) B cells were un-

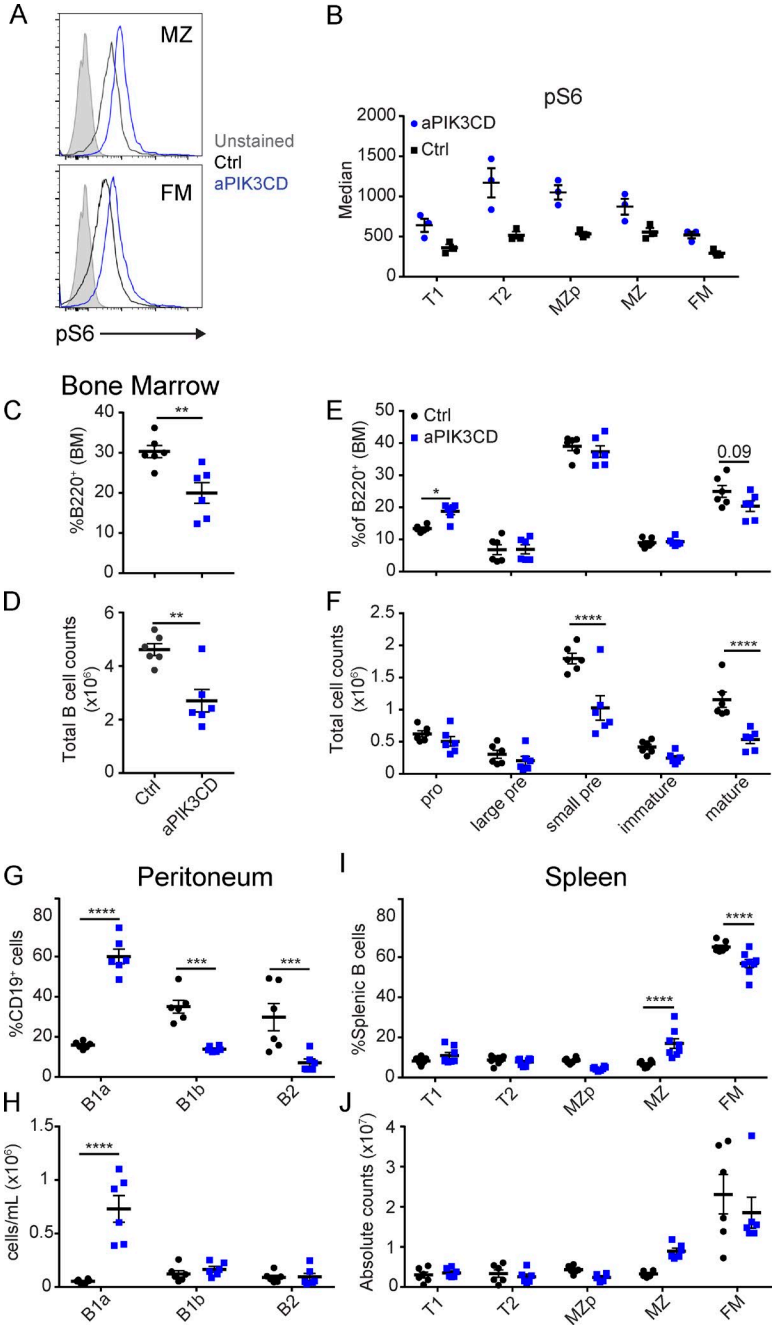

Figure 1. **Mb1-aPIK3CD mice exhibit BM B lymphopenia and expanded peripheral, innate B cell compartments. (A)** pS6 in unstimulated MZ (top) and FM (bottom) splenic B cells. Filled gray histogram: unstained control; open histograms: black, control, and blue, Mb1-aPIK3CD. **(B)** Median fluorescent intensity of pS6 in splenic B cell subsets in Mb1-aPIK3CD and control mice. Data shown are representative of one of two independent experiments with six controls and six Mb1-aPIK3CD mice. **(C and D)** Frequency (P = 0.006; C) and absolute cell counts (D) of BM B cells (B220+, P = 0.002) in littermate control (Ctrl) and Mb1-aPIK3CD mice. Significance calculated by Student's unpaired *t* test. **(E and F)** Frequency (pro–B cells, P = 0.03; E) and absolute cell counts (F) of BM B cell subsets (as defined in Fig. S1 E; small pre P, < 0.0001; mature P, < 0.0001). **(G and H)** Frequency (B1a, P < 0.0001; B1b, P = 0.0005; and B2, P = 0.0002; G) and absolute number (H) of peritoneal B cell subsets per milliliter of peritoneal fluid collected (as defined in Fig. S1 F; B1a, P < 0.0001). **(I and J)** Frequency (MZ and FM, P < 0.0001; I) and absolute number (J) of splenic B cell subsets (as defined in Fig. S1 G). (C–J) Black: control mice—animals expressing WT *Pik3cd*. Blue: aPIK3CD mice—mice expressing one copy of *Pik3cd-E1020K* (hE1021K) restricted to B cell lineage. **(E–J)** Significance calculated by two-way ANOVA. **(C–H)** Data representative of two independent experiments with six controls and six aPIK3CD mice all ∼12 wk of age. (I and J) Data representative of three independent experiments with six controls and eight aPIK3CD mice all ∼12 wk of age. *, P < 0.05; **, P < 0.01; ***, P < 0.001; ****, P < 0.0001. For summary graphs, lines indicate mean ± SEM.

changed in CD21-aPIK3CD mice (Fig. 2, J and K). Thus, restricting aPIK3CD expression to peripheral B cell stages is sufficient to drive expansion of innate B cell populations. Of note, a study (published during revision of our work) used a CRISPR/Cas9 generated p110δ^{E1020K} model to assess the impact of the identical genetic change on murine B cell development and reported increased numbers of splenic T1 B cells (B220$^+$CD93$^+$CD23$^-$) in the setting of global aPIK3CD expression and using BM chimera models (Avery et al., 2018). The discrepancy between this and our data may reflect use of alterative markers to define transitional B cells, as well as differences between a global knock-in versus B cell–intrinsic models. Notably, interaction with CD40L-expressing cells impacts transitional B cell development (Schwartz et al., 2014); thus, hyperactive PI3K signaling in other lineages or elevated B cell–activating factor (BAFF) levels in BM chimeras may help drive the expansion of T1 B cells. While we did not identify a numerical increase, we observed a trend of competitive advantage in aPIK3CD-expressing transitional B cells and, consistent with our data in both splenic and peritoneal compartments, the CRISPR-p110δ^{E1020K} model also identified increased innate B cell populations in the spleen.

Together with findings in the Mb1-aPIK3CD model, the decrease in recirculating, FM, and peritoneal B2 B cells supports the idea that aPIK3CD leads to B cell lymphopenia, as observed in APDS subjects, via a combined impact on BM development and reduced fitness of mature B2 B cells. Of note, B cell lymphopenia in APDS subjects is associated with a proportional, but not a numerical, increase in circulating transitional B cells and a

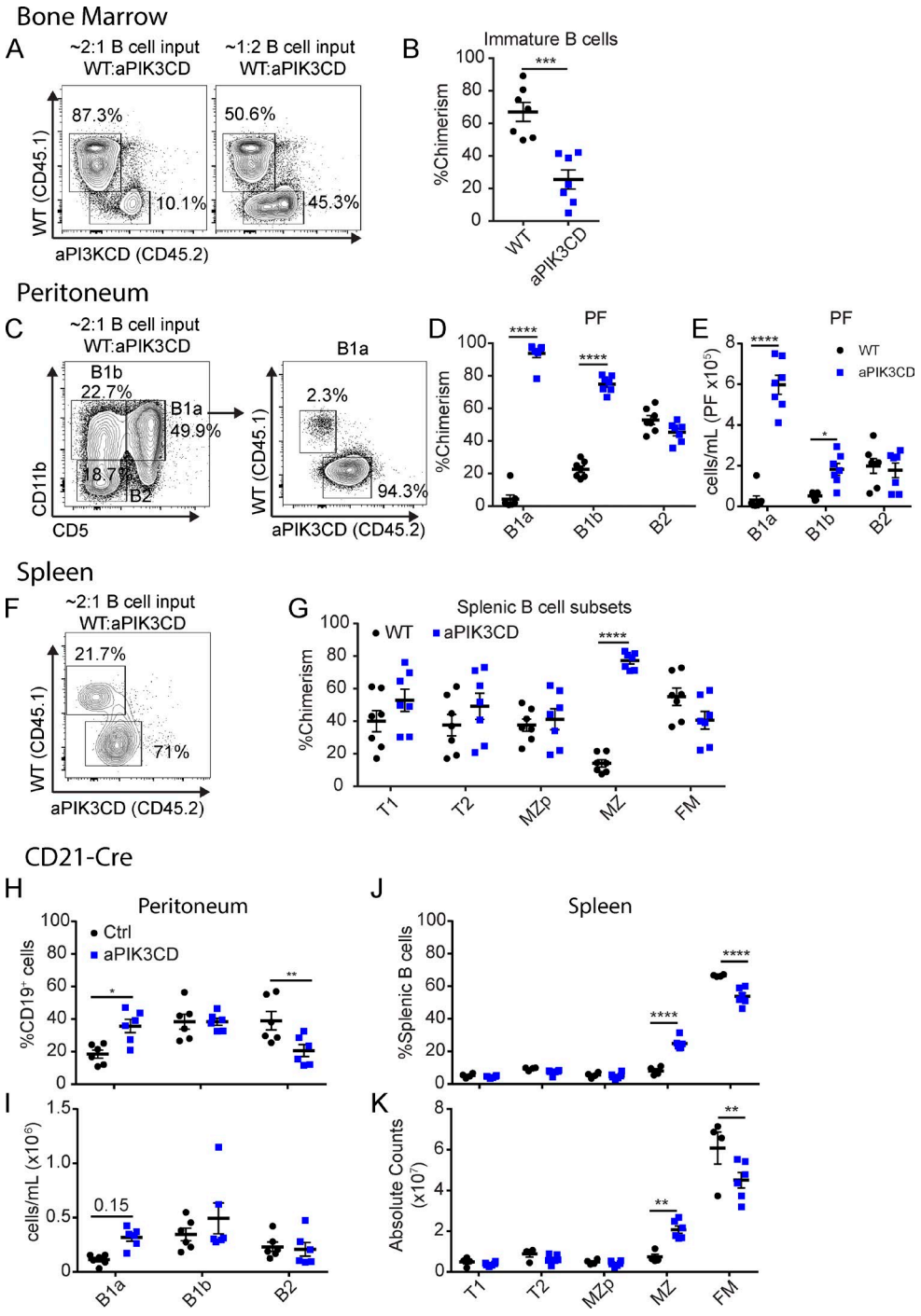

Figure 2. **aPIK3CD B cells exhibit a competitive disadvantage in the BM but outcompete WT B cells in innate B cell compartments. (A–G)** WT (CD45.1⁺) and Mb1-aPIK3CD (CD45.2⁺) total BM was adoptively transferred into preconditioned (CD45.1⁺/CD45.2⁺) µMT recipient animals. Recipient animals were sacrificed 12 wk after transfer. **(A)** Representative flow plots of BM B cell chimerism at 12 wk after transfer with left panel showing experiment using 2:1 ratio of WT to Mb1-aPIK3CD input BM B cells and right panel showing 1:2 ratio of WT to Mb1-aPIK3CD input BM B cells. **(B)** Immature BM B cell chimerism (P = 0.0003). Significance calculated by Student's unpaired *t* test. **(C)** Representative flow plots of peritoneal B cell subsets (left panel) and B1a B cell chimerism (right panel) at 12 wk after transfer of 2:1 ratio of WT to Mb1-aPIK3CD input BM B cells. **(D)** Chimerism of peritoneal B cell subsets (B1a and B1b, P < 0.0001). **(E)** Absolute number of peritoneal B cells derived from Mb1-aPIK3CD and WT donor BM (B1a, P < 0.0001; B1b, P = 0.02). **(F)** Representative flow plots of splenic MZ B cell chimerism at 12 wk after transfer of 2:1 ratio of WT to Mb1-aPIK3CD input BM B cells. **(G)** Chimerism of splenic B cell subsets (MZ, P < 0.0001). **(H–K)** aPIK3CD carrier animals were crossed to the CD21-Cre strain and characterized at ~12 wk of age. **(H and I)** Frequency (B1a, P = 0.01; B2, P = 0.008; H) and absolute numbers (I) of peritoneal B cell subsets per milliliter of peritoneal fluid collected. **(J and K)** Frequency (MZ and FM, P < 0.0001; J) and absolute numbers (K) of splenic B cell subsets (MZ, P = 0.005; FM, P = 0.0008). **(D, E, and G–K)** Significance calculated by two-way ANOVA. **(A and B)** Data representative of two independent experiments with seven recipients with input BM ratio as shown in A. **(C–G)** Data representative of two independent experiments with seven recipients with 2:1 ratio of WT to Mb1-aPIK3CD input BM B cells. **(H–K)** Data representative of two independent experiments with six controls and six CD21-aPIK3CD mice, 10–12 wk of age. *, P < 0.05; **, P < 0.01; ***, P < 0.001; ****, P < 0.0001. For summary graphs, lines indicate mean ± SEM.

reduction in the number of mature and memory B cells (Angulo et al., 2013; Lucas et al., 2014, 2016; Wentink et al., 2017). While we did not assess memory cells, our findings are consistent with these data where transitional B cell numbers were minimally impacted, while FM and recirculating B cells were numerically and proportionally reduced.

aPIK3CD does not alter cycling but differentially impacts immature versus innate B cell survival

To clarify how aPIK3CD leads to reduced BM B cells and higher B1a and MZ B cell numbers, we quantified its effects on cell proliferation and survival. To measure proliferation, Mb1-aPIK3CD and control mice were injected 24 h before sacrifice with BrdU, a thymidine analogue incorporated into DNA during S phase. We observed no difference in $BrdU^+$ BM B cell subsets in Mb1-aPIK3CD versus control mice (Fig. 3 A and Fig. S2 A). In the periphery, splenic B cell subsets including MZ B cells (Fig. 3 B) and peritoneal B2 (Fig. 3 C) showed no differences in cycling in Mb1-aPIK3CD mice compared with controls. In contrast, aPIK3CD B1a B cells exhibited decreased proliferation, and B1b cells showed a similar trend (Fig. 3 C).

Because there is no evidence of altered cycling under homeostatic conditions, we postulated that the reduction in immature B cells and/or expansion of innate B cells reflected differences in cell survival. Analysis of WT versus aPIK3CD B cells in the chimeric setting demonstrated an increased frequency of aPIK3CD-expressing immature B cells undergoing apoptosis ($TUNEL^+$; Fig. 3, D and E). Splenic MZ B cells exhibited diminished apoptosis in the chimeric setting, despite being more apoptotic before BM egress (Fig. 3 F). Under homeostatic conditions, removing the impact of hyperactive PI3K signaling in the BM, we observed decreased $TUNEL^+$ B1a B cells in CD21-aPIK3CD mice (Fig. 3 G) and similar trends in MZp and MZ B cells (data not shown). Consistent with these data, MZ B cells and peritoneal B cells exhibited decreased Annexin V staining, an alternative measure of apoptosis (Fig. S2, B–E). Together, these data show that B cell–intrinsic aPIK3CD expression promotes innate B cell survival without altering proliferation. Conversely, aPIK3CD expression limits survival of immature B cells, and may be selected against, without impacting proliferation.

Additional work is required to understand the contrasting impact of aPIK3CD in BM versus innate B cell development. Mice homozygous for catalytically inactive p110δ exhibit reduced numbers of BM pre–B and immature B cells (Okkenhaug et al., 2002), and deletion of both p110α and p110δ results in a more severe pre–B cell developmental arrest (Ramadani et al., 2010). Conversely, B cell–intrinsic Pdk1 deficiency also negatively impacts these BM B cell populations, with a near complete loss of recirculating and immature B cells due to a decreased frequency of pre–B cells (Baracho et al., 2014). Consistent with the idea that both reduced and enhanced PI3K activity may negatively impact BM B cell survival, PTEN deletion in pre–B cells expressing oncogenic BCR-ABL1 drives rapid leukemic cell death. This leads to down-regulation of IL-7R, CD19, and components of the pre-BCR and hyperactive Akt signaling, events that are countered by pharmacological inhibition of Akt (Shojaee et al., 2016). Thus, together with these previous data, our findings imply that altered PI3K signals dysregulate the pre-B checkpoint, leading to increased cell death, possibly via dysregulation of Pax5 target gene expression (Abdelrasoul et al., 2018). In the periphery, loss of PIK3CD restricts both MZ and B1a B cell development. In contrast, increased PI3K activity limits BCR-mediated apoptosis in splenic B cells, promoting survival and proliferation (Cheng et al., 2009). Additionally, PIK3CD is required for BAFF receptor–driven positive selection (Henley et al., 2008). As BAFF signals preferentially regulate innate B cell populations including B1 and MZ B cells, aPIK3CD may augment this BCR-dependent program, promoting innate cell expansion despite its negative impact on BM lymphopoiesis.

aPIK3CD expression drives plasma cell formation that correlates with elevated natural IgM

To assess the impact of aPIK3CD on immunoglobulin production and terminal differentiation, we quantified plasma cell numbers and antibody isotypes. We observed a significant increase in frequency and number of splenic plasma cells ($B220^-CD138^+$) in the absence of immunization (Fig. 4, A and B). In chimeras, we found that aPIK3CD B cells out-competed WT B cells in the germinal center (GC; $B220^+CD95^{hi}CD38^{lo}$) and plasma cell compartments (Fig. 4, C and D; and Fig. S2 F), supporting the idea that hyperactive PI3K signaling enhances terminal differentiation.

To further investigate the functional impact of alterations in plasma cells, B1a, and MZ B cells, we quantified serum antibody. Mb1-aPIK3CD mice exhibited an approximately threefold increase in both IgM and IgG3 (Fig. 4 E). Restricting expression of aPIK3CD to peripheral B cells also resulted in an increase in serum IgM and IgG3 (Fig. 4 G). B1 B cells are the major source of IgM and IgG3 natural antibodies that recognize self- and nonself/microbial antigens (Durand et al., 2009). Many natural antibodies recognize oxidation-specific epitopes on lipids and apoptotic cells. We found that MDA-LDL and phosphorylcholine (PC)-reactive (PC(10)) IgM were increased (Fig. 4 F) and reactivity to nuclear antigens was reduced (Fig. S2, G and H) in Mb1-aPIK3CD compared with control animals. Restriction of aPIK3CD expression to peripheral B cells led to a similar phenotype (Fig. 4, G and H). In addition, both models also showed increased, or a trend for increased, IgG reactivity for oxidized/natural antigens (Fig. S2 I). These findings suggest that hyperactive PI3K enhances the formation of plasma cells, which are derived, at least in part, by activation of innate B cells, leading to increased serum levels of natural antibodies.

Consistent with our findings in mice, APDS subjects exhibit increased circulating plasmablasts and elevated serum IgM (Angulo et al., 2013; Lucas et al., 2014, 2016; Wentink et al., 2017), implying that expansion of innate B cells may account for the common hyper-IgM phenotype. Assessment of IgM specificities in APDS subjects may provide important insight into this question. While B1a B cells have been proposed to generate natural IgM in murine models (Lalor et al., 1989; Chou et al., 2009; Holodick et al., 2010; Choi et al., 2012), analysis of BM IgM^+ plasma cells and peritoneal cell transfer studies suggests that an early B1 progenitor may preferentially seed the natural IgM^+ plasma cell compartment (Reynolds et al., 2015). To test this idea, we quantified B1 progenitors in the BM and observed sig-

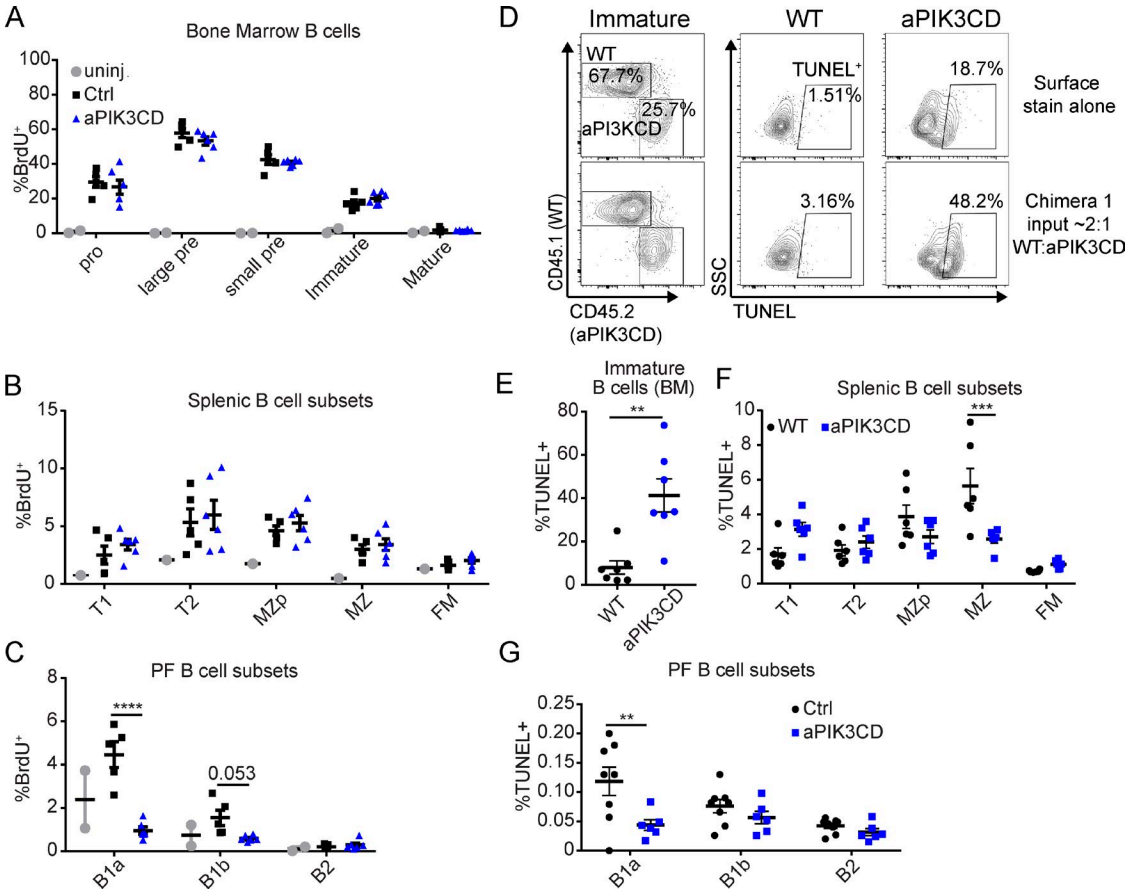

Figure 3. **aPIK3CD does not alter B cell cycling but differentially impacts survival in immature versus innate B cell subsets. (A–C)** Mb1-aPIK3CD and control mice were injected with 1 mg BrdU i.p. 24 h before sacrifice. Percent BrdU$^+$ cells in BM B cell subsets (A), percent BrdU$^+$ cells in splenic B cell subsets (B), and percent BrdU$^+$ cells in peritoneal B cell subsets (C) in Mb1-aPIK3CD and control mice (B1a, $P < 0.0001$). Data representative of two independent experiments with six controls and six Mb1-aPIK3CD mice injected with BrdU and two BrdU–uninjected control mice (12–30 wk of age); significance calculated by two-way ANOVA. **(D)** Representative flow plots from competitive chimera animals assessing cell survival in immature BM B cells. Plots shown depict the following: left panels, the relative frequency of WT (CD45.1) versus Mb1-aPIK3CD (CD45.2) immature BM B cells (B220$^+$IgM$^+$IgD$^-$); bottom, middle, and right panels, the frequency of apoptotic cells (TUNEL$^+$) within WT versus Mb1-aPIK3CD immature B cells, respectively; and top, middle, and right panels, WT versus Mb1-aPIK3CD immature B cells, respectively, not subjected to TUNEL staining shown as a negative control. **(E)** Percent TUNEL$^+$ WT versus Mb1-aPIK3CD BM immature B cells in µMT recipient animals ($P = 0.002$, 12 wk after transfer with 2:1 and 1:2 ratio of WT to Mb1-aPIK3CD input BM B cells; see Fig. 2 A). Significance calculated by Student's unpaired *t* test. Data representative of two independent experiments with seven recipients with input BM ratio as shown in Fig. 2 A. **(F)** Percent TUNEL$^+$ WT versus Mb1-aPIK3CD splenic B cell subsets in µMT recipient animals (MZ, $P = 0.0002$, 12 wk after transfer with same input as in D). Data representative of two independent experiments with seven recipients with 2:1 ratio of WT to Mb1-aPIK3CD input BM B cells. **(G)** Percent TUNEL$^+$ cells in peritoneal B cell subsets in CD21-aPIK3CD and control mice (B1a, $P = 0.002$, eight control and six CD21-aPIK3CD mice, 12–19 wk of age). **(F and G)** Significance calculated by two-way ANOVA. **, $P < 0.01$; ***, $P < 0.001$; ****, $P < 0.0001$. For summary graphs, lines indicate mean ± SEM.

nificant increases in their number and proportion (Fig. S3, A–C) in aPIK3CD mice (Montecino-Rodriguez et al., 2006). In future studies, aPIK3CD models could be used to define these progenitors and assess other B1 B cell functions, including generation of IL-10–producing subsets.

B cell–intrinsic aPIK3CD expression blunts TI immune responses

The elevated IgM and innate B cell numbers in aPIK3CD mice suggested these mice might exhibit an increased TI immune response. To test this hypothesis, we immunized Mb1-aPIK3CD and control mice with the TI antigen, NP-Ficoll. Despite increased basal NP-specific IgM, 7 d after immunization, Mb1-aPIK3CD mice had reduced NP-specific IgM compared with controls (Fig. 5, A and B). The fold change in antigen-specific IgM was also reduced (~1.4-fold versus ~6.5-fold in controls). Mb1-aPIK3CD mice also exhibited decreased NP-specific IgG3 at baseline and after immunization (Fig. S3, D and E). Notably, APDS patients suffer from recurrent sinopulmonary infections with encapsulated bacteria (*Streptococcal pneumonia* and *Haemophilus influenzae*) and exhibit diminished responses to polysaccharide-based vaccines (Angulo et al., 2013; Lucas et al., 2014, 2016). To test whether aPIK3CD mice exhibit a defective response to polysaccharide antigens, we immunized control and Mb1-aPIK3CD mice with Pneumovax23 (PPV23) and measured antibody titers at 6 and 12 d after immunization. Similar to alterations in mice immunized with NP-Ficoll, Mb1-aPIK3CD mice exhibited higher baseline levels of antigen-specific IgM (Fig. S3 F). While peak IgM antibody titers were similar to controls (Fig. 5 C), the overall fold-induction of antigen-specific antibody was re-

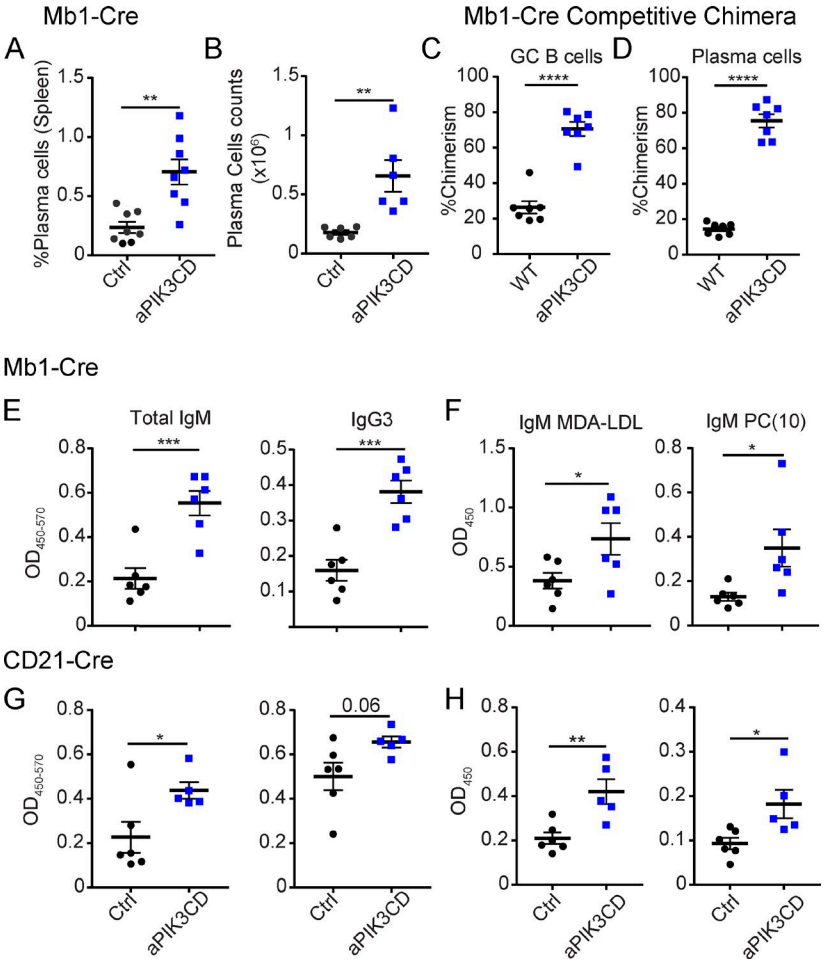

Figure 4. **aPIK3CD enhances plasma cell differentiation and IgM and IgG3 production in the absence of immunization. (A and B)** Frequency (P = 0.001; A) and absolute number (B) of plasma cells ($B220^{-}CD138^{+}$) in the spleen of unimmunized Mb1-aPIK3CD and control mice (P = 0.005). **(C and D)** Chimerism of GC ($B220^{+}CD95^{hi}CD38^{lo}$, P < 0.0001) B cells (C) and plasma cells (P < 0.0001; D) in the spleen of µMT recipient animals (12 wk after transfer with 2:1 ratio of WT versus Mb1-aPIK3CD input BM B cells). **(E)** Optical density of serum IgM (left panel, P = 0.0009) and IgG3 (right panel, P = 0.0005) in control versus Mb1-aPIK3CD mice. **(F)** Optical density of serum MDA-LDL–specific (left panel, P = 0.04) and PC(10)-specific IgM (right panel, P = 0.03) in control versus Mb1-aPIK3CD mice. **(G)** Optical density of serum IgM (left panel, P = 0.03) and IgG3 (right panel) in control versus CD21-aPIK3CD mice. **(H)** Optical density of serum MDA-LDL–specific (left panel, P = 0.004) and PC(10)-specific IgM (right panel, P = 0.02) in control versus CD21-aPIK3CD mice. Significance calculated by unpaired Student's *t* test. **(A, B, E, and F)** Data representative of two independent experiments with six controls versus six Mb1-aPIK3CD mice. **(C and D)** Data representative of two independent experiments with seven µMT recipient animals. **(G and H)** Data representative of two independent experiments with six controls versus six CD21-aPIK3CD mice. Controls were Cre-negative littermates at 18 wk of age. *, P < 0.05; **, P < 0.01; ***, P < 0.001; ****, P < 0.0001. For summary graphs, lines indicate mean ± SEM.

duced ~1.5–2-fold in the Mb1-aPIK3CD mice (Fig. 5 D). Thus, B cell–intrinsic aPIK3CD expression blunts the capacity to mount a TI immune response. While the precise mechanism responsible for this defective response remains to be determined, the increased number of innate B cells and elevated baseline levels of antigen-specific IgM suggest that antibody-forming cells derived from antigen-triggered, aPIK3CD innate B cells exhibit reduced survival and/or other functional changes that limit sustained TI antibody production.

B cell–intrinsic aPIK3CD expression skews GCs toward a light zone (LZ) fate and limits Ig class-switching

Patients with APDS exhibit defects in circulating, class-switched memory B cells, and normal or reduced serum IgG, with preferential loss of IgG2 (Angulo et al., 2013; Lucas et al., 2014, 2016; Wentink et al., 2017). Lymph node biopsies have revealed either increased or decreased GC B cell follicles with normal or reduced IgG-positive cells (Crank et al., 2014; Lucas et al., 2014; Elkaim et al., 2016). IgG and IgA transcripts exhibit minimal differences in activation-induced cytidine deaminase (AID) targeting and somatic hypermutation (Wentink et al., 2017), and in in vitro studies, primary B cells from APDS patients revealed either normal or reduced production of class-switched antibodies (Crank et al., 2014; Chiriaco et al., 2017). Together, these previous observations suggest that aPIK3CD expression may inhibit class-switch recombination in human B cells. Similarly, alternative mouse models of GC-restricted hyperactive PI3K signaling exhibit defective class-switch recombination (Dominguez-Sola et al., 2015; Sander et al., 2015). To directly assess how aPIK3CD impacts a TD immune response, we challenged mice with virus-like particles (VLPs) containing a TLR7 ligand. To eliminate any impact of aPIK3CD on B cell development or BCR repertoire, we performed studies using the AID-Cre strain. In this model, aPIK3CD expression is induced upon transcription of AID, which is most highly expressed in GC B cells (Victora et al., 2012). At 14 d after VLP immunization, we observed no differences in the frequency of total or VLP-specific GC B cells (Fig. 5, E–G). GC B cell–intrinsic deletion of FOXO1 (Dominguez-Sola et al., 2015) or constitutive activation of PI3K (p110α; Sander et al., 2015) results in a reduction of the GC dark zone (DZ) compartment. Consistent with these previous findings, GC B cells in AID-aPIK3CD mice demonstrated skewing toward an LZ ($CXCR4^{-}CD86^{+}$) phenotype (Fig. 5, H and I). To determine how aPIK3CD impacts the production of antigen-specific antibodies, we measured VLP-specific serum titers. At 14 d after immunization, AID-aPIK3CD mice exhibited a heightened VLP-specific IgM response compared with control animals (Fig. 5 J). In contrast, AID-aPIK3CD mice generated a blunted class-switched response with reduced levels of VLP-specific total IgG and IgG2c, the dominant isotype triggered in response to VLP immunization (Fig. 5, K and L). To assess the impact of aPIK3CD when expressed

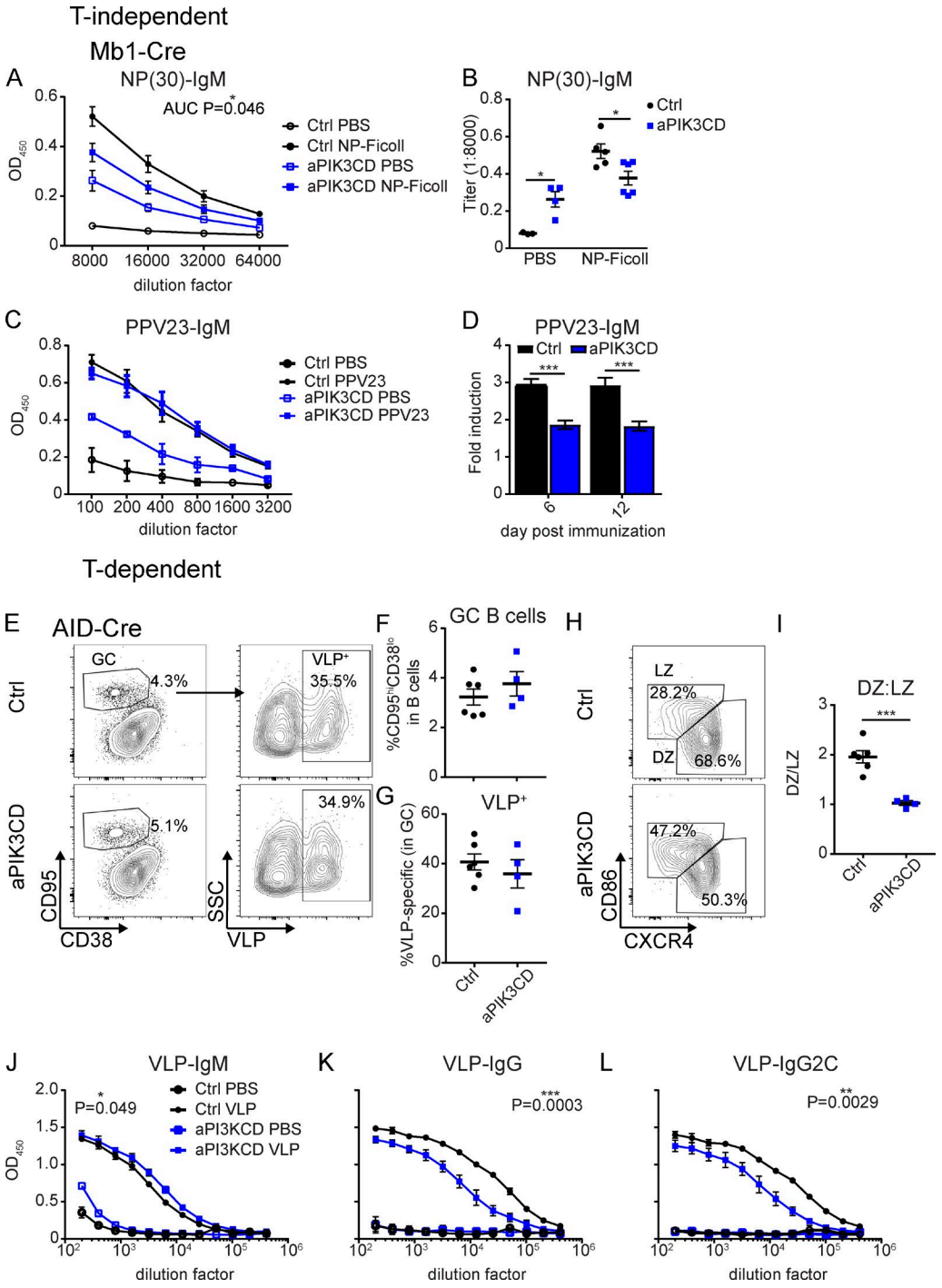

Figure 5. **B cell–intrinsic aPIK3CD expression limits both TI and TD humoral responses. (A and B)** Control and Mb1-aPIK3CD mice were injected i.p. with 50 µg NP-Ficoll or PBS and sacrificed 7 d after immunization. **(A)** Dilution curves of low-affinity (NP-30) antigen-specific IgM in serum at 7 d after immunization. Significance calculated by Student's *t* test, testing area under the curve (AUC; P = 0.046) with baseline of 0.0415. Open black circles: control injected with PBS; filled black circles: control injected with NP-Ficoll; open blue squares: Mb1-aPIK3CD injected with PBS; filled blue squares: Mb1-aPIK3CD injected with NP-Ficoll. **(B)** End point titers of low-affinity (NP-30) antigen-specific IgM at 1:8,000 serum dilution (PBS, P = 0.02; and NP-Ficoll, P = 0.02). Significance calculated by Student's *t* test. (A and B) Data representative of two independent experiments with three control mice injected with PBS and five injected with NP-Ficoll, and four Mb1-aPIK3CD mice injected with PBS and six injected with NP-Ficoll. **(C and D)** Control and Mb1-aPIK3CD mice were injected i.p. with 0.125 µg PPV23 or PBS. **(C)** Dilution curves of PPV23-specific IgM in serum at 6 d after immunization. Black open circles: control PBS–injected (n = 2); black filled circles: control PPV23–injected (n = 7); blue open squares: Mb1-aPIK3CD PBS–injected (n = 2); blue filled squares: Mb1-aPIK3CD PPV23–injected (n = 5). **(D)** Fold induction of PPV23-IgM over baseline (day 0) OD_{450} for days 6 and 12 after immunization with PPV23 (day 6, P = 0.0004; day 12, P = 0.0003). Black: control PPV23–injected mice; blue: Mb1-aPIK3CD PPV23–injected mice. Significance calculated by two-way ANOVA. Data representative of two independent experiments with mice 19–21 wk of age. **(E–L)** Control and AID-aPIK3CD mice were injected i.p. with PBS or 2 µg of VLPs containing TLR7 ligand in 250 µl and sacrificed 14 d after immunization. **(E)** Representative flow plots of GC B cells ($B220^+CD95^{hi}CD38^{lo}$; left) and VLP-specific cells (VLP^+; right) within the GC at 14 d after immunization. Top panels: control; bottom panels: AID-aPIK3CD. **(F and G)** Frequency of GC B cells (F) and VLP-specific cells (G) in GC at 14 d after

in all peripheral B cell populations, we performed identical immunization studies using CD21-aPIK3CD mice (Fig. S3, G–L). We observed a modest increase in the proportion of GC B cells with a decrease in the proportion of VLP-specific cells, LZ skewing, and reduced levels of VLP-specific total IgG and IgG2c in CD21-aPIK3CD compared with control animals. Thus, consistent with previous observations in APDS subjects and in alternative mouse models of activated PI3K, B cell–intrinsic aPIK3CD promotes GC LZ cell skewing and limits, but does not eliminate, class-switch recombination of antigen-specific B cells.

In summary, we describe a robust, Cre-inducible model to assess lineage-specific impact of aPIK3CD expression. Using intercross with a series of B lineage–specific Cre strains, we demonstrate that aPIK3CD expression in B cells is sufficient for several features of APDS including elevated IgM, reduced responses to both TI and TD antigens, and discrete alterations in the BM and peripheral B cell compartments. Further, our data indicate that a subset of these clinical findings likely reflects alterations in innate B cell compartments that warrant direct assessment in patients. To date, no information is available regarding splenic MZ structures and, while all subjects in one study had an increased proportion of $CD5^+CD20^+$ B cells (Lucas et al., 2014), direct assessment of candidate human B1 populations (Griffin et al., 2011) in peripheral or, ideally, tissue compartments may be informative. Finally, a key finding in our study is that while the innate B cell compartment is increased in aPIK3CD animals, these cells are unable to manifest normal TI responses. This finding likely explains the near universal failure of APDS subjects to respond to the polyvalent pneumococcal vaccine and, at least in part, the recurrent sinopulmonary infections in these subjects with *S. pneumoniae*. Notably, a recent study using the oral PI3K-delta inhibitor leniolisib in six APDS patients demonstrated improvement in disease features including reduction in serum IgM, normalization of the peripheral blood B cell phenotype, and reduced adenopathy (Dornan et al., 2017). Together with our findings, these observations suggest that combining leniolisib with delivery of pneumococcal vaccine may provide improved protection from *S. pneumoniae* in these patients, an idea that could be initially assessed in the animal model described here. Finally, while aPIK3CD increases the risk for multiple forms of B cell lymphoma (Kracker et al., 2014), PI3K-delta inhibitors may also increase the risk for genomic instability in malignant B cells (Compagno et al., 2017), suggesting that long-term use of these agents may need to be carefully assessed in this context.

Materials and methods

Mice

$Mb1^{Cre/+}$, $CD21^{Cre/+}$, $AID^{Cre/Cre}$, and μMT mice were bred and maintained in the specific pathogen-free animal facility of Seattle Children's Research Institute and handled according to Institutional Animal Care and Use Committee–approved protocols. aPIK3CD mice were generated by knock-in of mutant exon 24 bearing E1020K in 3′→5′ orientation downstream of endogenous exon 24, flanked by loxp sites as shown in Fig. S1 A. The targeting vector also included a neo-cassette flanked by frt sites in the endogenous PIK3CD locus that was removed by intercross with Flp-strain mice (ACTB:FLPe B6J mice; Jackson Laboratories) following germline transmission. aPIK3CD mice were subsequently crossed to various B cell–specific Cre-bearing strains as described to induce excision of endogenous exon 24 and expression of mutant exon 24, via Cre-mediated double-stranded breaks at the indicated Loxp and mLoxp sites, resulting in fixing the inversion in place as previously described (Fig. S1 A; Mullally et al., 2010). $Mb1^{Cre/+}$ mice were provided by M. Reth (Max Planck Institute of Immunobiology, Freiburg, Germany). All aPIK3CD mice in this study are heterozygous for the E1020K mutation, and all control animals are Cre-negative littermates.

Immunization

16–30-wk-old mice were i.p. immunized with 50 μg of NP-Ficoll (Biosearch Technologies) in 200 μl. For VLP immunization, mice 12–18 wk of age were injected i.p. with 2 μg/250 μl VLPs or 250 μl 1× PBS. VLPs were provided by B. Hou (Chinese Academy of Sciences, Beijing, China). For PPV23 (Merck) injection, mice were injected with 0.125 μg/200 μl i.p. per mouse or 200 μl 1× PBS.

ddPCR assay

ddPCR assays were performed in a total volume of 25 μl. Each reaction contained 50 ng of gDNA with a final 1× ddPCR Supermix for probes (Bio-Rad), 900 nM primers and 250 nM of each reference (labeled with hexachlorofluorescein [HEX]) and junction (labeled with fluorescein [FAM]) probes. Droplets containing this reaction mix were generated (Bio-Rad QX200 ddPCR droplet generator) and amplified by PCR with the following thermocycler conditions: one cycle of 95°C for 10 min; 40 cycles of 95°C for 30 s, 60°C for 30 s, and 72°C for 30 s; one cycle of 98°C for 10 min; and holding at 12°C. Amplified samples were analyzed on the QX200 Droplet Reader (Bio-Rad) using the QuantaSoftTM software (Bio-Rad). In order to define the positive droplets in the HEX and FAM channels, the same threshold was applied to all samples for each probe. Thereafter, to calculate flipping frequency, FAM-positive droplets of junction probe were divided by HEX-positive droplets of reference probe. Primers used for amplification are as follows: PI3K-Fw: 5′-AACCCGTACCCAACAAACAT-3′; and PI3K-Rev: 5′-GCTAACGAAGAGAGGGACAC-3′. Probes used for measuring flipped and unflipped amplification products are as follows: reference probe: 5′-(HEX)CCTGCGGCTACTGACACGAC(BHQ1)-3′; and knock-in/junction probe: 5′-(FAM)ACCTCAGGGAGGGAC AGAATGGACCCC(BHQ1)-3′.

immunization. Black: control; blue: AID-aPIK3CD. **(H)** Representative flow plots of DZ ($CXCR4^+CD86^-$) versus LZ ($CXCR4^-CD86^+$) GC B cells from control (top) and AID-aPIK3CD (bottom) mice at 14 d after immunization. **(I)** Ratio of DZ:LZ within GC in control (black) versus AID-aPIK3CD (blue) mice (P = 0.0003). Significance calculated by Student's *t* test. **(J and K)** Dilution curves of serum VLP-specific IgM (P = 0.049; J), IgG (P = 0.0003; K), and IgG2C (P = 0.0029; L). P value calculated by Student's *t* test of AUC (baseline of 0). **(E–L)** Data representative of two independent experiments with six control mice injected with VLPs and two injected with PBS, and four AID-aPIK3CD mice injected with VLPs and two injected with PBS at 13–16 wk of age. *, P < 0.05; **, P < 0.01; ***, P < 0.001. For summary graphs and dilution curves, lines indicate mean ± SEM. For the bar graph, error bars indicate mean + SEM.

Reagents

LIVE/DEAD Fixable Near-IR Dead Cell Stain Kit (Invitrogen) was used according to the manufacturer's instructions. Alexa Fluor 350 carboxylic acid, succinyl ester (Invitrogen) was used according to the manufacturer's instructions. Anti-murine antibodies used in the study include the following: CD45.1 (A20), CD38 (90), IgM (II/41), CD8 (53–6.7), Gr-1/Ly-6G (RB6-8C5), and SA-e450 from eBioscience; IgD (11–26), BP-1 (FG35.4), and λ (JC5-1) from Southern Biotech; B220 (RA3-6B2), CD19 (6D5), CD24 (M1/69), CD21 (7E9 and 7G6), CD23 (B3B4), BP-1 (6C3), and CD4 (GK1.5) from Biolegend; CD45.2 (104), CD43 (S7), CD21 (7G6), CD19 (1D3), CD138 (281–2), CD95/Fas (Jo2), IgG1 (A85-1), κ (187.1), CXCR4 (2B11), CD86 (GL1), CD11b (M1/70), CD5 (53–7.3), and SA-PE from BD Biosciences; CD3 (500A2), SA-AF700, and SA-APC from Life Technologies; and PNA from Vector Laboratories. VLP-specific B cell detection ex vivo was performed as previously described (Hou et al., 2011).

Competitive chimera BM transplantations

BM was harvested from donor WT (CD45.1) and Mb1-aPIK3CD (CD45.2), and single-cell suspensions were mixed at a 50:50 ratio for retro-orbital injection of 5×10^6 cells into lethally irradiated (900 cGy) μMT (CD45.1/CD45.2) recipients. Resulting BM chimeras were sacrificed 12–14 wk after transplantation. Data are representative of two independent experiments.

Flow-cytometric analysis

Single-cell suspensions from spleen, BM, and peritoneal fluid (PF) were obtained as previously described (Becker-Herman et al., 2011) and incubated with fluorescence-labeled antibodies for 15 min at 4°C. For phospho-flow analysis, 1×10^6 cells were fixed with fix/permeabilization solution (BD Biosciences) for 20 min at room temperature (RT) in the dark. Cells were resuspended in 90% methanol and stored at −20°C for a minimum of 30 min. Cells were washed with FACS buffer (1× PBS plus 2% FBS) twice and stained for surface and phospho-site antibodies for 45 min at RT in the dark. Data were collected on an LSRII (BD Biosciences) and analyzed using FlowJo software (Tree Star).

Cell cycle analysis

For in vivo labeling of cycling cells, mice were i.p. injected with 1 mg BrdU 24 h before sacrifice. Both spleen and BM were collected, and cells were surface stained, fixed, permeabilized, treated with DNase for 1 h at 37°C, and stained with anti-BrdU FITC (BrdU kit from BD Biosciences). Data were collected on an LSRII (BD Biosciences) and analyzed using FlowJo software (Tree Star).

ELISA

To test total serum Ig titers, 96-well Nunc-Immuno MaxiSorp plates (Thermo Fisher Scientific) were precoated overnight at 4°C with 2 μg/ml anti-IgM, anti-IgG, anti-IgG1, anti-IgG2C, and anti-IgG3. For total Ig ELISAs, serum was diluted 1:6,250, 1:31,250, and 1:156,250. Serum diluted at 1:200 was tested for reactivity to double-stranded DNA (Sigma-Aldrich), Smith-ribonucleoproteins (ATRO1-10; Arotech Diagnostics Limited), and MDA-LDL (20P-MD L-105; Academy Biomedical) at 100 μg/ml. To detect NP-specific antibody levels in serum, 96-well Nunc-Immuno MaxiSorp plates were coated with NP(30)-BSA (50 μg/ml; Biosearch Technologies) overnight at 4°C. Serum was diluted 1:8,000, 1:16,000, 1:32,000, and 1:64,000. To test reactivity to VLP, plates were coated with 1 μg/ml Qb VLP antigen, and serum was serially diluted twice from 1:200 to 1:409,600. To test reactivity to PPV23, plates were coated with 10 μg/ml Pneumovax, and serum was diluted 1:100. Plates were blocked for 1 h with 2% BSA in PBS before addition of diluted serum for 2 h at RT or overnight at 4°C. Specific antibodies were detected using goat anti-mouse IgM–, IgG–, IgG1–, or IgG3–horseradish peroxidase or rat anti-mouse IgG2C–horseradish peroxidase (1:2,000 dilution; SouthernBiotech). Peroxidase reactions were developed using OptEIA TMB substrate (BD Biosciences) and stopped with sulfuric acid. Absorbance at 450 nm was read using a SpectraMax 190 microplate reader (Molecular Devices). For total Ig titers, 450-nm absorbance was corrected by subtraction of 570-nm absorbance. For antigen-specific ELISAs, 450-nm absorbance was reported.

Apoptosis assays

Total cells from spleen, BM, and PF were incubated with fluorescently labeled antibodies for 30 min at 4°C in staining buffer, followed by TUNEL-based apoptosis analysis. Cells were fixed overnight at 4°C in 2% paraformaldehyde, permeabilized for 2 min on ice in permeabilization solution (0.1% TritonX-100 and 0.1% sodium citrate), and labeled according to the manufacturer's instructions (In Situ Cell Death Detection kit, Fluorescein; Sigma-Aldrich). Data were collected using an LSR II and analyzed using FlowJo software. For Annexin V staining, total cells from spleen or PF were incubated with fluorescently labeled antibodies for 15 min at 4°C in staining buffer, followed by Annexin V staining with a dead cell apoptosis kit (Life Technologies). Cells were resuspended in 1× Annexin-binding buffer and stained with Annexin V 488 for 15 min at RT in the dark. The reaction was quenched with 1× Annexin-binding buffer, and samples were run immediately on an LSRII (BD Biosciences) and analyzed using FlowJo software (Tree Star).

Statistical analysis

Unpaired two-tailed Student's *t* tests were applied to assess statistical significance of the differences between groups of mice. For experiments that have more than two groups, more than two treatments or more than two time points, one- or two-way ANOVA was used to assess group and treatment differences, and the Bonferroni method was used to correct for multiple hypotheses in pairwise comparisons. The P values were considered significant when $P < 0.05$ (*), $P < 0.01$ (**), $P < 0.001$ (***), and $P < 0.0001$ (****).

Online supplemental material

Fig. S1 shows Cre recombinase–mediated excision events proceed by two paths resulting in excision of endogenous exon 24 and inversion and expression of mutant exon 24. Expression of mutant exon 24 is restricted to B cells and absent in $CD4^+$ T cells in the CD21-aPIK3CD model with expected allelic frequency, representative gating strategy for BM, peritoneal, and splenic B cell subsets. Fig. S2 shows incorporation of BrdU into B cell subsets in the BM under homeostatic conditions, Annexin V staining in splenic B cells, Annexin V staining in peritoneal B cells, an advantage

for Mb1-aPIK3CD–derived cells within the GC and splenic plasma cell compartments in the competitive BM chimeras, diminished nuclear antigen reactive IgM in Mb1-aPIK3CD mice compared with controls, and total IgG reactivity to MDA-LDL and PC(10) in Mb1-aPIK3CD and CD21-aPIK3CD mice compared with controls. Fig. S3 shows increased B1 progenitor B cells in the BM of Mb1-aPIK3CD mice compared with controls, decreased NP(30)-IgG3 at 7 d after NP-Ficoll immunization of Mb1-aPIK3CD mice compared with controls, increased PPV23 reactive IgM at baseline and comparable titers after immunization in Mb1-aPIK3CD mice compared with controls, and mild increase in total GC B cells with decreased antigen-specific (VLP specific) cells within the GC of CD21-aPIK3CD mice, with increased LZ skewing of the GC and decreased class-switched VLP-specific antibodies compared with controls 14 d after immunization.

Acknowledgments

We would like to thank Kerri Thomas, Tanvi Arkatkar, and Socheath Khim for advice and assistance with experimental procedures, experimental design, and mouse colony maintenance.

This work was supported by the National Institutes of Health under award numbers T32AI106677 (MNWD), DP3-DK097672 (D.J. Rawlings), DP3-DK111802 (D.J. Rawlings), and R01CA201135 (R.G. James). Additional support was provided by a Cancer Research Institute Training Grant (MND), the Children's Guild Association Endowed Chair in Pediatric Immunology (D.J. Rawlings), and the Benaroya Family Gift Fund (D.J. Rawlings). The content is solely the responsibility of the authors and does not necessarily represent the official views of the National Institutes of Health.

The authors declare no competing financial interests.

Author contributions: M. Wray-Dutra, F.A. Qureshah, and G. Metzler designed, performed, and interpreted experiments. M. Oukka and D.J. Rawlings designed the murine model. R.G. James and D.J. Rawlings designed the overall study and interpreted data. M. Wray-Dutra generated figures, and M. Wray-Dutra, F.A. Qureshah, R.G. James, and D.J. Rawlings wrote the manuscript.

Submitted: 29 March 2018
Revised: 5 July 2018
Accepted: 16 August 2018

References

Abdelrasoul, H., M. Werner, C.S. Setz, K. Okkenhaug, and H. Jumaa. 2018. PI3K induces B-cell development and regulates B cell identity. *Sci. Rep.* 8:1327. https://doi.org/10.1038/s41598-018-19460-5

Angulo, I., O. Vadas, F. Garçon, E. Banham-Hall, V. Plagnol, T.R. Leahy, H. Baxendale, T. Coulter, J. Curtis, C. Wu, et al. 2013. Phosphoinositide 3-kinase δ gene mutation predisposes to respiratory infection and airway damage. *Science.* 342:866–871. https://doi.org/10.1126/science.1243292

Avery, D.T., A. Kane, T. Nguyen, A. Lau, A. Nguyen, H. Lenthall, K. Payne, W. Shi, H. Brigden, E. French, et al. 2018. Germline-activating mutations in *PIK3CD* compromise B cell development and function. *J. Exp. Med.* 215:2073–2095. https://doi.org/10.1084/jem.20180010

Baracho, G.V., M.H. Cato, Z. Zhu, O.R. Jaren, E. Hobeika, M. Reth, and R.C. Rickert. 2014. PDK1 regulates B cell differentiation and homeostasis. *Proc. Natl. Acad. Sci. USA.* 111:9573–9578. https://doi.org/10.1073/pnas.1314562111

Becker-Herman, S., A. Meyer-Bahlburg, M.A. Schwartz, S.W. Jackson, K.L. Hudkins, C. Liu, B.D. Sather, S. Khim, D. Liggitt, W. Song, et al. 2011. WASp-deficient B cells play a critical, cell-intrinsic role in triggering autoimmunity. *J. Exp. Med.* 208:2033–2042. https://doi.org/10.1084/jem.20110200

Browning, M.J., A. Chandra, V. Carbonaro, K. Okkenhaug, and J. Barwell. 2015. Cowden's syndrome with immunodeficiency. *J. Med. Genet.* 52:856–859. https://doi.org/10.1136/jmedgenet-2015-103266

Cheng, S., C.Y. Hsia, B. Feng, M.L. Liou, X. Fang, P.P. Pandolfi, and H.C. Liou. 2009. BCR-mediated apoptosis associated with negative selection of immature B cells is selectively dependent on Pten. *Cell Res.* 19:196–207. https://doi.org/10.1038/cr.2008.284

Chiriaco, M., I. Brigida, P. Ariganello, S. Di Cesare, G. Di Matteo, F. Taus, D. Cittaro, D. Lazarevic, A. Scarselli, V. Santilli, et al. 2017. The case of an APDS patient: Defects in maturation and function and decreased in vitro anti-mycobacterial activity in the myeloid compartment. *Clin. Immunol.* 178:20–28. https://doi.org/10.1016/j.clim.2015.12.008

Choi, Y.S., J.A. Dieter, K. Rothaeusler, Z. Luo, and N. Baumgarth. 2012. B-1 cells in the bone marrow are a significant source of natural IgM. *Eur. J. Immunol.* 42:120–129. https://doi.org/10.1002/eji.201141890

Chou, M.Y., L. Fogelstrand, K. Hartvigsen, L.F. Hansen, D. Woelkers, P.X. Shaw, J. Choi, T. Perkmann, F. Bäckhed, Y.I. Miller, et al. 2009. Oxidation-specific epitopes are dominant targets of innate natural antibodies in mice and humans. *J. Clin. Invest.* 119:1335–1349. https://doi.org/10.1172/JCI36800

Compagno, M., Q. Wang, C. Pighi, T.C. Cheong, F.L. Meng, T. Poggio, L.S. Yeap, E. Karaca, R.B. Blasco, F. Langellotto, et al. 2017. Phosphatidylinositol 3-kinase δ blockade increases genomic instability in B cells. *Nature.* 542:489–493. https://doi.org/10.1038/nature21406

Conley, M.E., A.K. Dobbs, A.M. Quintana, A. Bosompem, Y.D. Wang, E. Coustan-Smith, A.M. Smith, E.E. Perez, and P.J. Murray. 2012. Agammaglobulinemia and absent B lineage cells in a patient lacking the p85α subunit of PI3K. *J. Exp. Med.* 209:463–470. https://doi.org/10.1084/jem.20112533

Crank, M.C., J.K. Grossman, S. Moir, S. Pittaluga, C.M. Buckner, L. Kardava, A. Agharahimi, H. Meuwissen, J. Stoddard, J. Niemela, et al. 2014. Mutations in PIK3CD can cause hyper IgM syndrome (HIGM) associated with increased cancer susceptibility. *J. Clin. Immunol.* 34:272–276. https://doi.org/10.1007/s10875-014-0012-9

Dominguez-Sola, D., J. Kung, A.B. Holmes, V.A. Wells, T. Mo, K. Basso, and R. Dalla-Favera. 2015. The FOXO1 Transcription Factor Instructs the Germinal Center Dark Zone Program. *Immunity.* 43:1064–1074. https://doi.org/10.1016/j.immuni.2015.10.015

Dornan, G.L., B.D. Siempelkamp, M.L. Jenkins, O. Vadas, C.L. Lucas, and J.E. Burke. 2017. Conformational disruption of PI3Kδ regulation by immunodeficiency mutations in *PIK3CD* and *PIK3R1*. *Proc. Natl. Acad. Sci. USA.* 114:1982–1987. https://doi.org/10.1073/pnas.1617244114

Dulau Florea, A.E., R.C. Braylan, K.T. Schafernak, K.W. Williams, J. Daub, R.K. Goyal, J.M. Puck, V.K. Rao, S. Pittaluga, S.M. Holland, et al. 2017. Abnormal B-cell maturation in the bone marrow of patients with germline mutations in PIK3CD. *J. Allergy Clin. Immunol.* 139:1032–1035.e6. https://doi.org/10.1016/j.jaci.2016.08.028

Durand, C.A., K. Hartvigsen, L. Fogelstrand, S. Kim, S. Iritani, B. Vanhaesebroeck, J.L. Witztum, K.D. Puri, and M.R. Gold. 2009. Phosphoinositide 3-kinase p110 delta regulates natural antibody production, marginal zone and B-1 B cell function, and autoantibody responses. *J. Immunol.* 183:5673–5684. https://doi.org/10.4049/jimmunol.0900432

Elkaim, E., B. Neven, J. Bruneau, K. Mitsui-Sekinaka, A. Stanislas, L. Heurtier, C.L. Lucas, H. Matthews, M.C. Deau, S. Sharapova, et al. 2016. Clinical and immunologic phenotype associated with activated phosphoinositide 3-kinase δ syndrome 2: A cohort study. *J. Allergy Clin. Immunol.* 138:210–218.e9. https://doi.org/10.1016/j.jaci.2016.03.022

Griffin, D.O., N.E. Holodick, and T.L. Rothstein. 2011. Human B1 cells in umbilical cord and adult peripheral blood express the novel phenotype CD20+ CD27+ CD43+ CD70-. *J. Exp. Med.* 208:67–80. https://doi.org/10.1084/jem.20101499

Henley, T., D. Kovesdi, and M. Turner. 2008. B-cell responses to B-cell activation factor of the TNF family (BAFF) are impaired in the absence of PI3K delta. *Eur. J. Immunol.* 38:3543–3548. https://doi.org/10.1002/eji.200838618

Hobeika, E., S. Thiemann, B. Storch, H. Jumaa, P.J. Nielsen, R. Pelanda, and M. Reth. 2006. Testing gene function early in the B cell lineage in mb1-cre mice. *Proc. Natl. Acad. Sci. USA.* 103:13789–13794. https://doi.org/10.1073/pnas.0605944103

Holodick, N.E., J.R. Tumang, and T.L. Rothstein. 2010. Immunoglobulin secretion by B1 cells: differential intensity and IRF4-dependence of sponta-

neous IgM secretion by peritoneal and splenic B1 cells. *Eur. J. Immunol.* 40:3007–3016. https://doi.org/10.1002/eji.201040545

Hou, B., P. Saudan, G. Ott, M.L. Wheeler, M. Ji, L. Kuzmich, L.M. Lee, R.L. Coffman, M.F. Bachmann, and A.L. DeFranco. 2011. Selective utilization of Toll-like receptor and MyD88 signaling in B cells for enhancement of the antiviral germinal center response. *Immunity*. 34:375–384. https://doi.org/10.1016/j.immuni.2011.01.011

Jou, S.T., N. Carpino, Y. Takahashi, R. Piekorz, J.R. Chao, N. Carpino, D. Wang, and J.N. Ihle. 2002. Essential, nonredundant role for the phosphoinositide 3-kinase p110delta in signaling by the B-cell receptor complex. *Mol. Cell. Biol.* 22:8580–8591. https://doi.org/10.1128/MCB.22.24.8580-8591.2002

Kracker, S., J. Curtis, M.A. Ibrahim, A. Sediva, J. Salisbury, V. Campr, M. Debré, J.D. Edgar, K. Imai, C. Picard, et al. 2014. Occurrence of B-cell lymphomas in patients with activated phosphoinositide 3-kinase δ syndrome. *J. Allergy Clin. Immunol.* 134:233–236. https://doi.org/10.1016/j.jaci.2014.02.020

Lalor, P.A., L.A. Herzenberg, S. Adams, and A.M. Stall. 1989. Feedback regulation of murine Ly-1 B cell development. *Eur. J. Immunol.* 19:507–513. https://doi.org/10.1002/eji.1830190315

Liu, Q., A.J. Oliveira-Dos-Santos, S. Mariathasan, D. Bouchard, J. Jones, R. Sarao, I. Kozieradzki, P.S. Ohashi, J.M. Penninger, and D.J. Dumont. 1998. The inositol polyphosphate 5-phosphatase ship is a crucial negative regulator of B cell antigen receptor signaling. *J. Exp. Med.* 188:1333–1342. https://doi.org/10.1084/jem.188.7.1333

Lucas, C.L., H.S. Kuehn, F. Zhao, J.E. Niemela, E.K. Deenick, U. Palendira, D.T. Avery, L. Moens, J.L. Cannons, M. Biancalana, et al. 2014. Dominant-activating germline mutations in the gene encoding the PI(3)K catalytic subunit p110δ result in T cell senescence and human immunodeficiency. *Nat. Immunol.* 15:88–97. https://doi.org/10.1038/ni.2771

Lucas, C.L., A. Chandra, S. Nejentsev, A.M. Condliffe, and K. Okkenhaug. 2016. PI3Kδ and primary immunodeficiencies. *Nat. Rev. Immunol.* 16:702–714. https://doi.org/10.1038/nri.2016.93

Martin, F., and J.F. Kearney. 2001. B1 cells: similarities and differences with other B cell subsets. *Curr. Opin. Immunol.* 13:195–201. https://doi.org/10.1016/S0952-7915(00)00204-1

Montecino-Rodriguez, E., H. Leathers, and K. Dorshkind. 2006. Identification of a B-1 B cell-specified progenitor. *Nat. Immunol.* 7:293–301. https://doi.org/10.1038/ni1301

Mullally, A., S.W. Lane, B. Ball, C. Megerdichian, R. Okabe, F. Al-Shahrour, M. Paktinat, J.E. Haydu, E. Housman, A.M. Lord, et al. 2010. Physiological Jak2V617F expression causes a lethal myeloproliferative neoplasm with differential effects on hematopoietic stem and progenitor cells. *Cancer Cell.* 17:584–596. https://doi.org/10.1016/j.ccr.2010.05.015

Okada, H., S. Bolland, A. Hashimoto, M. Kurosaki, Y. Kabuyama, M. Iino, J.V. Ravetch, and T. Kurosaki. 1998. Role of the inositol phosphatase SHIP in B cell receptor-induced Ca2+ oscillatory response. *J. Immunol.* 161:5129–5132.

Okkenhaug, K., A. Bilancio, G. Farjot, H. Priddle, S. Sancho, E. Peskett, W. Pearce, S.E. Meek, A. Salpekar, M.D. Waterfield, et al. 2002. Impaired B and T cell antigen receptor signaling in p110delta PI 3-kinase mutant mice. *Science.* 297:1031–1034.

Ramadani, F., D.J. Bolland, F. Garcon, J.L. Emery, B. Vanhaesebroeck, A.E. Corcoran, and K. Okkenhaug. 2010. The PI3K isoforms p110alpha and p110delta are essential for pre-B cell receptor signaling and B cell development. *Sci. Signal.* 3:ra60. https://doi.org/10.1126/scisignal.2001104

Reynolds, A.E., M. Kuraoka, and G. Kelsoe. 2015. Natural IgM is produced by CD5- plasma cells that occupy a distinct survival niche in bone marrow. *J. Immunol.* 194:231–242. https://doi.org/10.4049/jimmunol.1401203

Sander, S., V.T. Chu, T. Yasuda, A. Franklin, R. Graf, D.P. Calado, S. Li, K. Imami, M. Selbach, M. Di Virgilio, et al. 2015. PI3 Kinase and FOXO1 Transcription Factor Activity Differentially Control B Cells in the Germinal Center Light and Dark Zones. *Immunity.* 43:1075–1086. https://doi.org/10.1016/j.immuni.2015.10.021

Schwartz, M.A., N.S. Kolhatkar, C. Thouvenel, S. Khim, and D.J. Rawlings. 2014. CD4+ T cells and CD40 participate in selection and homeostasis of peripheral B cells. *J. Immunol.* 193:3492–3502. https://doi.org/10.4049/jimmunol.1400798

Shojaee, S., L.N. Chan, M. Buchner, V. Cazzaniga, K.N. Cosgun, H. Geng, Y.H. Qiu, M.D. von Minden, T. Ernst, A. Hochhaus, et al. 2016. PTEN opposes negative selection and enables oncogenic transformation of pre-B cells. *Nat. Med.* 22:379–387. https://doi.org/10.1038/nm.4062

Victora, G.D., D. Dominguez-Sola, A.B. Holmes, S. Deroubaix, R. Dalla-Favera, and M.C. Nussenzweig. 2012. Identification of human germinal center light and dark zone cells and their relationship to human B-cell lymphomas. *Blood.* 120:2240–2248. https://doi.org/10.1182/blood-2012-03-415380

Wentink, M., V. Dalm, A.C. Lankester, P.A. van Schouwenburg, L. Schölvinck, T. Kalina, R. Zachova, A. Sediva, A. Lambeck, I. Pico-Knijnenburg, et al. 2017. Genetic defects in PI3Kδ affect B-cell differentiation and maturation leading to hypogammaglobulineamia and recurrent infections. *Clin. Immunol.* 176:77–86. https://doi.org/10.1016/j.clim.2017.01.004

Zhang, K., A. Husami, R. Marsh, and M.B. Jordan. 2013. Identification of a phosphoinositide 3 kinase (PI 3K p110? (PIK3CD) deficient individual. *J. Clin. Immunol.* 33:673–674.